Escola de Primavera de Transição e Turbulência
Blumenau 2022

ABCM
13th Spring School on Transition and Turbulence
September 19th-23rd, 2022, Blumenau, SC, Brazil

EPTT-2022-0001
A STUDY ON THE EFFECTS OF MESH REFINEMENT FOR TRANSITIONAL FLOWS INCLUDING CROSSFLOW-TRIGGERED TRANSITION

Aline R. Santos Righi
Instituto Tecnológico de Aeronáutica, 12228-900, São José dos Campos, SP, Brazil
alinerighi29@gmail.com

Gustavo Luiz Olichevis Halila
Embraer S. A., Research & Development, 12227-901, São José dos Campos, SP, Brazil
gustavo.halila@embraer.com.br

João Luiz F. Azevedo
Instituto de Aeronáutica e Espaço, 12228-904, São José dos Campos, SP, Brazil
joaoluiz.azevedo@gmail.com

Abstract. *Computational Fluid Dynamics (CFD) techniques have been used for many decades now in many different applications for academic or industrial purposes. The CFD methods have been used in the aerospace industry, for example, for design and development process for some time now. However, the appropriate treatment of the laminar-turbulent transition is still a challenge and requires further research. Here, we use the Langtry-Menter transition model coupled with the SST model for turbulence closure. The Langtry-Menter transition model is composed of two additional transport equations to predict laminar-turbulent transition. Many mechanisms can trigger transition, for instance, the amplification of Tollmien-Schlichting waves and bypass transition. The original Langtry-Menter transition was capable of predicting both mechanisms through the use of empirical correlations. More recently, additional empirical correlations were proposed to predict transition caused by stationary crossflow vortices. One of such correlations accounts for the surface roughness. The main test case addressed here is the flow over a prolate spheroid. The present work presents a study on the effects of mesh refinement and numerical parameter settings on the numerical results. Our goal is to identify guidelines leading to accurate crossflow-triggered transition to turbulence computations.*

Keywords: *Laminar-Turbulent Transition, Langtry-Menter Transition Model, Mesh Refinement, Empirical Correlations, Crossflow Instabilities*

1. INTRODUCTION

Transitional flows are relevant in the aerospace industry. The NASA CFD vision 2030 study (Slotnick *et al.*, 2014) suggests that transitional flow modeling capabilities are relevant to leverage the aerodynamicist ability to used CFD as an effective design tool. In order to correctly treat the laminar-turbulent transition, Computational Fluid Dynamics (CFD) tools have been used for many different purposes in the academic and industry. Despite that, the correct treatment of the laminar-turbulent transition remains a challenge. For the last years, many modeling strategies were published to deal with transitional flows through an e^n method or an empirical correlation. However, some of the available methods do not include all the necessary effects of transition or represent high computational costs. For example, the approaches available based on the stability equations with an e^n method (Smith and Gamberoni, 1956; van Ingen, 1956) are not compatible with general-purposes CFD methods. These methods employ the stability equations coupled with a CFD code (Halila *et al.*, 2019), resulting in a complex framework with, at least, three different codes: a boundary layer generation tool, a flow stability analysis module and a CFD code.

The low-Re models are compatible with modern CFD codes (Jones and Launder, 1973). However, they typically suffer from a close interaction with the transition capability and the viscous sublayer modeling, which can prevent an independent calibration of both phenomena (Savill, 1993, 1996). Also, these models are not usually applicable for complex geometries (Halila, 2014). Standard correlation-based methodologies present several technical challenges. For example, in aerodynamics applications the edge of the boundary layer is not well defined and the need for performing simulations based on unstructured grids in parallelized CFD codes is another challenge (Halila, 2014). Also, the Reynolds-averaged Navier-Stoles (RANS) equations are based on a time-averaging procedure, and therefore, only an average frequency is seen by the model and important spectral information is lost (Halila *et al.*, 2016). The conventional RANS methods do not account for transitional flows, where both linear and nonlinear effects are relevant.

Unlike the other approaches, modified RANS models were proposed with the idea of allowing accurate and inexpensive transitional flow predictions. These models use a standard, fully-turbulent RANS model with one or two additional

transport equations based on local parameters and empirical correlations. With these concepts in mind, the Langtry-Menter transition model (Langtry and Menter, 2009) (LCTM - Local Correlation-based Transition Model) was proposed. The Langtry-Menter transition model is composed of two transport equations, one for the intermittency and one for the transition momentum thickness Reynolds number (Langtry and Menter, 2009). Moreover, the Langtry-Menter model uses empirical correlations for the correct prediction of the different mechanisms of transition.

Transition can be triggered through different mechanisms. For instance, the amplification of Tollmien-Schlichting (TS) waves (Klebanoff *et al.*, 1962), bypass transition (Ghasemi *et al.*, 2014), crossflow vortices (Saric and Dagenhart, 1999), and leading edge transition and flow contamination (Poll, 1978) are the most common. The first published Langtry-Menter transition model (Langtry and Menter, 2009) represents transition caused by the amplification of TS waves and bypass transition, but not transition due to stationary crossflow vortices. As a consequence, many extensions of the model were proposed and published in the literature during the last years. One of these extensions accounts for an empirical correlation for the stationary crossflow vortices based on the surface roughness (Langtry *et al.*, 2015).

The Langtry-Menter model was implemented in an in-house code, BRU3D (Bigarella, 2007; Bigarella and Azevedo, 2009; Carvalho *et al.*, 2018). However, transition caused by stationary crossflow vortices was not considered. In this paper, we consider an empirical correlation for stationary crossflow vortices published in Langtry *et al.* (2015), and the empirical correlation is implemented in the BRU3D code. We present a study with the prolate spheroid test case on the freestream turbulence intensity variable considering transition due to TS waves, and a study on the mesh refinement for the stationary crossflow vortices.

2. METHODOLOGY

For the development of the present work, an in-house developed CFD code, BRU3D (Bigarella, 2007; Bigarella and Azevedo, 2007; Carvalho *et al.*, 2018), is used. The BRU3D code has been continuously improved by the research group through the years. The code can solve the compressible Euler equations and/or the RANS equations. One of the implemented turbulence models in the code is the Shear Stress Transport (SST) (Menter, 1994) model. For transition, the Langtry-Menter laminar-turbulent transition model (Langtry and Menter, 2009) is also implemented. Results that demonstrated the validation of the code can be found in Refs. Bigarella and Azevedo (2007); Bigarella (2007). In the BRU3D code, the equations are solved in a standard, cell-centered, finite-volume method for spatial discretization (Hirsh, 1990) for unstructured grids (Bigarella, 2007; Bigarella and Azevedo, 2009). The code can be executed using parallel MPI calls. Further information can be found in Refs. Bigarella and Azevedo (2009); Carvalho (2018).

2.1 The Shear Stress Transport Turbulence Model

In our implementation, the Langtry-Menter $\gamma - Re_\theta$ transition model (Langtry and Menter, 2009) is coupled to the SST turbulence model (Menter, 1994). The SST model is based on the Boussinesq hypothesis, in which the eddy viscosity, μ_t, is used as a means to represent the Reynolds stress tensor terms. The SST model uses a blending function, F1, to combine the advantages of the k-ϵ and the k-ω models. The blending function, F1, activates the k-ω model in the near wall region, and the k-ϵ model for the rest of the flow. The SST model is composed of two equations. The first equation is for the turbulent kinetic energy, k, given by

$$\frac{\partial(\rho k)}{\partial t} + \frac{\partial(\rho u_j\, k)}{\partial x_j} = P_k - D_k + \frac{\partial}{\partial x_j}\left[\left(\mu + \frac{\mu_t}{\sigma_k}\right)\frac{\partial k}{\partial x_j}\right], \tag{1}$$

where ρ is the density, u_j represents the velocity vector components, P_k is the production term and D_k is the destruction term, μ is the molecular dynamic viscosity, μ_t is the eddy viscosity, and $\sigma_k = 0.85$. The second equation is for the turbulence frequency, ω, given by

$$\frac{\partial(\rho\omega)}{\partial t} + \frac{\partial(\rho u_j\omega)}{\partial x_j} = \frac{\gamma}{\nu_t}P_\omega - \beta\rho\omega^2 + \frac{\partial}{\partial x_j}\left[\left(\mu + \frac{\mu_t}{\sigma_k}\right)\frac{\partial\omega}{\partial x_j}\right] + (1-F_1)2\rho\sigma_{\omega 2}\frac{1}{\omega}\frac{\partial k}{\partial x_j}\frac{\partial\omega}{\partial x_j}, \tag{2}$$

where P_ω is the production term, $\beta = 0.09$, $\gamma = \frac{\beta_1}{\beta*} - \frac{\sigma_{\omega 1}\kappa^2}{\sqrt{\beta*}}$ with $\beta_1 = 0.075$, $\sigma_{\omega 1} = 0.5$ and $\kappa = 0.41$, and $\sigma_{\omega 2} = 0.856$.

The production term for the kinetic energy equations, P_k, is

$$P_k = \min\left(\mu_t S^2, 10D_k\right), \tag{3}$$

where S is the strain rate magnitude, given by

$$S = \sqrt{2S_{ij}S_{ij}}. \tag{4}$$

The destruction term for the kinetic energy equation, D_k, is

$$D_k = \beta^*\rho\omega k. \tag{5}$$

The blending function, F_1, is

$$F_1 = \tanh\left(\min\left(\max\left(\frac{\sqrt{k}}{\beta * \omega y}\,;\,\frac{500\nu}{y^2\omega}\right)\,;\,\frac{4\rho\sigma_{\omega 2}k}{CD_{k\omega}y^2}\right)\right)^4 , \tag{6}$$

where y is the distance from the field point to the nearest wall, and

$$CD_{k\omega} = \max\left(2\rho\sigma_{\omega 2}\frac{1}{\omega}\frac{\partial k}{\partial x_j}\frac{\partial \omega}{\partial x_j}\,;\,1\times 10^{-10}\right) . \tag{7}$$

The turbulent viscosity is calculated as follows

$$\mu_t = \min\left(\frac{\rho k}{\omega}\,;\,\frac{a_1\rho k}{SF_2}\right) , \tag{8}$$

where $a_1 = 0.31$. The F_2 term is a blending function given by

$$F_2 = \tanh\left\{\max\left(2\frac{\sqrt{k}}{\beta * \omega y}\,;\,\frac{500\mu_t}{\rho y^2\omega}\right)\right\}^2 . \tag{9}$$

Further information on the SST model can be found in Ref. Menter (1994).

2.2 Langtry-Menter Transition Model Standard Formulation

The Langtry-Menter $\gamma - Re_{\theta_t}$ transition model (Langtry and Menter, 2009) is coupled with the SST turbulence model (Menter, 1994) for the present work. The model is composed of two transport equations in addition to the equations for the SST model. The Langtry-Menter transition model is based only on local variables and is compatible with modern CFD codes. In the Langtry-Menter model, the strain rate Reynolds number, which is a local variable, maps the transition momentum-thickness Reynolds number, which is nonlocal and plays an important role in transition prediction. The transport equation for intermittency, γ, is given by

$$\frac{\partial(\rho\gamma)}{\partial t} + \frac{\partial(\rho u_j\gamma)}{\partial x_j} = P_\gamma - E_\gamma + \frac{\partial}{\partial x_j}\left[\left(\mu + \frac{\mu_t}{\sigma_f}\right)\frac{\partial\gamma}{\partial x_j}\right] , \tag{10}$$

where ρ is the density, u_j represents the velocity vector components, P_γ is the intermittency source term, E_γ is the destruction-relaminarization source term, μ is the molecular dynamic viscosity, μ_t is the eddy viscosity and $\sigma_f = 1.0$. The intermittency represents the probability of a fluid cell to be turbulent and is used to trigger the SST source terms. The second transport equation represents the transition momentum thickness Reynolds number, $\tilde{Re}_{\theta_t}$, and is given by

$$\frac{\partial\left(\rho\tilde{Re}_{\theta_t}\right)}{\partial t} + \frac{\partial\left(\rho u_j\tilde{Re}_{\theta_t}\right)}{\partial x_j} = P_{\theta_t} + \frac{\partial}{\partial x_j}\left[\sigma_{\theta_t}\left(\mu + \mu_t\right)\frac{\partial\tilde{Re}_{\theta_t}}{\partial x_j}\right] , \tag{11}$$

where P_{θ_t} is the source term and $\sigma_{\theta_t} = 2.0$ controls the diffusion coefficient. The Reynolds number based on the momentum-thickness represents a sensor responsible for triggering the transition process, because $\tilde{Re}_{\theta_t}$ indicates the point where transition begins. The Langtry-Menter model couples the intermittency function with the SST model to activate the turbulent kinetic energy,

$$\frac{\partial(\rho k)}{\partial t} + \frac{\partial(\rho u_j k)}{\partial x_j} = \tilde{P}_k - \tilde{D}_k + \frac{\partial}{\partial x_j}\left[\left(\mu + \sigma_k\mu_t\right)\frac{\partial k}{\partial x_j}\right] , \tag{12}$$

$$\tilde{P}_k = \gamma_{eff}P_k, \tag{13}$$

$$\tilde{D}_k = \min\left(\max\left(\gamma_{eff}\,,\,0.1\right)\,,\,1.0\right)D_k\,, \tag{14}$$

$$R_y = \frac{\rho y\sqrt{k}}{\mu}\,, \tag{15}$$

$$F_3 = \exp\left[-\left(\frac{R_y}{120}\right)^8\right] , \tag{16}$$

$$F_1 = \max(F_{1orig}, F_3)\,, \tag{17}$$

where $\tilde{P}_k$ and $\tilde{D}_k$ are the original production and destruction terms of the SST model, $\gamma_{eff}P_k$ includes the separation effects in the formulation, and F_{1orig} is the original SST blending function. The original Langtry-Menter transition model is able to predict transition triggered by the amplification of Tollmien-Schlichting waves and bypass transition through empirical correlations. Further information can be found in the literature Langtry and Menter (2009).

2.3 Empirical Correlation Based on the Surface Roughness

The Langtry-Menter transition model was extended to predict transition due to stationary crossflow transition. The empirical correlation (Langtry *et al.*, 2015) for crossflow effects is based on the streamwise vorticity ($\Omega_{\text{Streamwise}}$), alternatively known as helicity, as an indicator of the local crossflow strength in the boundary layer, defined as follows

$$\vec{U} = \left(\frac{u}{\sqrt{u^2+v^2+w^2}} , \frac{v}{\sqrt{u^2+v^2+w^2}} , \frac{w}{\sqrt{u^2+v^2+w^2}} \right) , \tag{18}$$

$$\vec{\Omega} = \left(\frac{\partial w}{\partial y} - \frac{\partial v}{\partial z} , \frac{\partial u}{\partial z} - \frac{\partial w}{\partial x} , \frac{\partial v}{\partial x} - \frac{\partial u}{\partial y} \right) , \tag{19}$$

$$\Omega_{Streamwise} = |\vec{U} \cdot \vec{\Omega}|. \tag{20}$$

In order to non-dimensionalize $\Omega_{\text{Streamwise}}$ into a measure of the crossflow strength, and to build an empirical correlation based on $H_{\text{crossflow}}$, the non-dimensional parameter is defined as

$$H_{Crossflow} = \frac{y \Omega_{Streamwise}}{U}, \tag{21}$$

as the crossflow strength indicator, where y is the distance to the nearest wall and U is the magnitude of the nondimensional velocity vector defined in Eq. (18). The empirical correlation for crossflow effects accounts for the surface roughness on the transition momentum thickness Reynolds number,

$$Re_{SCF} = \frac{\theta_t \rho \left(\frac{U}{0.82}\right)}{\mu} = -35.088 \ln\left(\frac{h}{\theta_t}\right) + 319.51 + f(+\Delta H_{crossflow}) - f(-\Delta H_{crossflow}) , \tag{22}$$

where $f(+\Delta H_{crossflow})$ and $f(-\Delta H_{crossflow})$ are a shift up or down depending on the local crossflow strength, θ_t is the momentum thickness, and U is the velocity magnitude. The crossflow effect is implemented as a stationary crossflow sink term D_{SCF}, in the Re_{θ_t} transport equation as

$$\frac{\partial(\rho \tilde{R}e_{\theta_t})}{\partial t} + \frac{\partial(\rho u_j \tilde{R}e_{\theta_t})}{\partial x_j} = P_{\theta_t} + D_{SCF} + \frac{\partial \left[\sigma_{\theta_t}(\mu + \mu_t)\frac{\partial \tilde{R}e_{\theta_t}}{\partial x_j}\right]}{\partial x_j}, \tag{23}$$

where

$$D_{SCF} = c_{\theta_t} \frac{\rho}{t} c_{Crossflow} \min\left(Re_{SCF} - \tilde{R}e_{\theta_t} , 0.0\right) (F_{\theta_t 2}) , \tag{24}$$

$$F_{\theta_t 2} = \min\left(F_{wake} e^{-\left(\frac{y}{\delta}\right)^4} , 1.0\right) , \tag{25}$$

where $c_{crossflow} = 0.6$ and $F_{\theta_t 2}$ confines the crossflow sink term D_{SCF} so that it is only activated inside the boundary layer. Further information on the details of the above empirical correlation can be found in the literature (Langtry *et al.*, 2015).

3. RESULTS AND DISCUSSIONS

The Langtry-Menter transition model that was originally implemented in the BRU3D code was validated and the results can be found in Carvalho (2018). After that, two test cases for zero-pressure gradient flat plates (Rumsey and Lee-Rausch, 2015; Coder, 2018) were addressed in a previous work. The first test accounts for transition due to Tollmien-Schlichting waves, which is characterized by a freestream turbulent intensity, Tu_i, lower than 1%. The second considers bypass transition, characterized by Tu_i larger than 1%. The test cases used a 5 million Reynolds number, a 0.2 Mach number, and three different meshes. Moreover, for transition due to TS waves, we also include a study on the simulation of the flow over the NLF(1)-0416 airfoil (Somers, 1981). The test case used a 4 million Reynolds number, a 0.2 Mach number, a zero-degree angle of attack, Tu_i of 0.15%, and 0.3%. The results included are for the skin friction coefficient, c_f, where it is possible to observe where the transition to turbulence starts. When inspecting c_f curves, it is usual to consider that transition to turbulence takes place in the region where the skin friction coefficient rises past its initial decrease in the laminar flow region. Further information can be found in Righi *et al.* (2021).

In the present paper, we discuss the numerical results of the c_f contours for the prolate spheroid test case. First, we present cases for which transition is triggered by the amplification of TS waves. The reference freestream parameters for the cases are summarized in Table 1. The 6:1 inclined spheroid was chosen as a validation test for the γ-Re_{θ_t} model with a comprehensive experimental study accomplished by the low speed wind tunnel DLR in Göttingen (Kreplin *et al.*, 1985). Various operational test conditions were considered in the experiments, including transition only due to Tollmien-Schlichting instabilities, transition caused by both Tollmien-Schlichting and crossflow instabilities, and transition dominated by crossflow instabilities. For the experimental cases, the freestream turbulence intensity in the wind tunnel was in the range of $Tu_\infty \approx 0.1\%$.

In Grabe and Krumbein (2013) a few operational test conditions for the transition cases mentioned before were considered for computations and confronted with the experimental results. The authors considered for the simulations a flow condition with a 1.5 millions Reynolds number, a 10-degree angle of attack, a Mach number of 0.03, a freestream turbulence intensity at the farfield boundary was set to $Tu_{ff} = 1.0\%$, and an eddy viscosity to molecular viscosity ratio, μ_t/μ_{ref}, of 5.0. These two parameters are fundamental quantities in the present modeling approach. The turbulent level of c_f is smaller in the computational than in the experiment for the transition caused by Tollmien-Schlichting waves, but the area of increasing c_f where indicates the transition region are in good agreement (Grabe and Krumbein, 2013). Later, our results are confronted with the results obtained in Kreplin *et al.* (1985) for the c_f contours through the white line in our own plots, which indicates the transition front extracted from the reference results.

Table 1. Freestream turbulent variables for transition due to the amplification of Tollmien-Schlichting waves cases.

Case	Re	Mach	α	T_u	μ_t/μ_{ref}	Mesh(Total nodes)
Case A	1.5×10^6	0.14	10 deg	0.2%	100	2,715,698
Case B	1.5×10^6	0.14	10 deg	0.1%	100	2,715,698
Case C	1.5×10^6	0.14	10 deg	0.5%	100	2,715,698

Figure 1 depicts our numerical results obtained with the BRU3D for Case A. The regions on the surface where the c_f contours shift from blue to yellow represent the transition location. Confronting our numerical results with the white line, representing the experimental data obtained from Kreplin *et al.* (1985), as mentioned before, we observe good agreement between the results. Moreover, Fig. 2 shows the residual convergence for the L-infinity norm for the four turbulent variables, k, ω, γ, and Re_{θ_t} for the results shown in Fig. 1. As mentioned before, this test consists of transition caused by the amplification of Tollmien-Schlichting waves using the freestream turbulence variables corresponding to the wind tunnel setup. It is possible to see that the equation for γ has the best convergence rate, while the equation for Re_{θ_t} has the lower convergence rate. Both equations for the SST model has similar convergence rates.

Figures 3 and 4 show the numerical results for the c_f contours obtained with the BRU3D code for Cases B and C, respectively. The main difference between them is the reference freestream turbulence intensity, Tu_i, which is our variable of interest. Case B considers the smallest value in the simulations for Tu_i, while Case C considers the largest value for Tu_i. One can see that, by changing the reference value of Tu_i, the results for Case B and Case C for the c_f contours are reduced with respect to Case A. However, the values for the c_f contours are similar confronting Case B and Case C, and the contours do not reveal any significant change between them. One can also observe that Case B and Case C present c_f contours levels slightly lower than the ones for Case A and the ones found in Langtry *et al.* (2015).

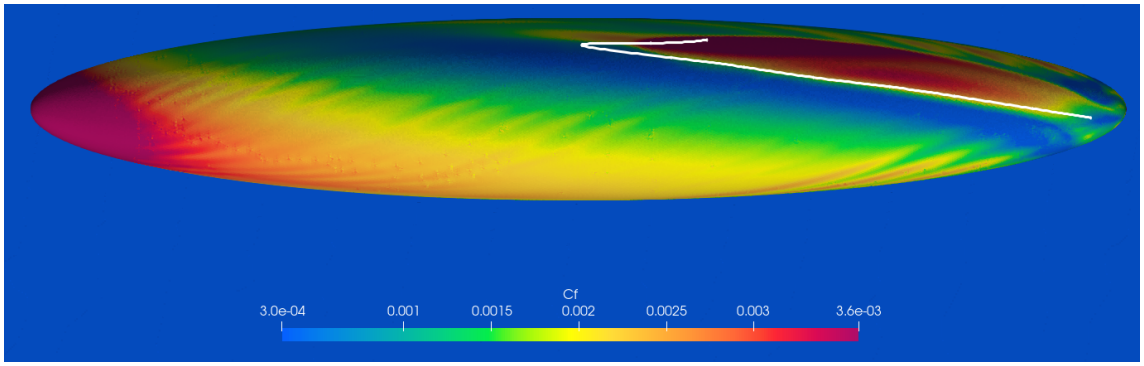

Figure 1. Skin friction coefficient contours for Case A.

We also include results for the newly implemented empirical correlation for stationary crossflow transition found in Langtry *et al.* (2015) for the prolate spheroid geometry. The investigations include the study on the impact in the numerical solutions for a mesh refinement test that aims to reproduce the stationary crossflow transition. Again, the experimental results are based on Ref. Kreplin *et al.* (1985) as mentioned before. For a Mach number of 0.136, a 15-degree angle of

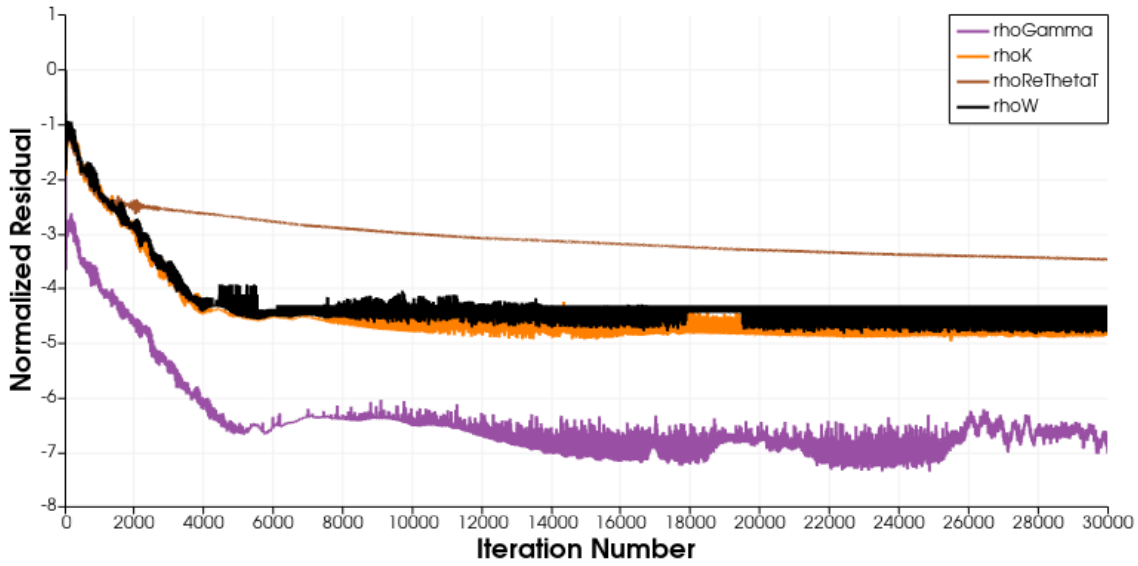

Figure 2. Residual convergence for the turbulent variables for the test case of transition due to the amplification of Tollmien-Schlichting waves in Case A.

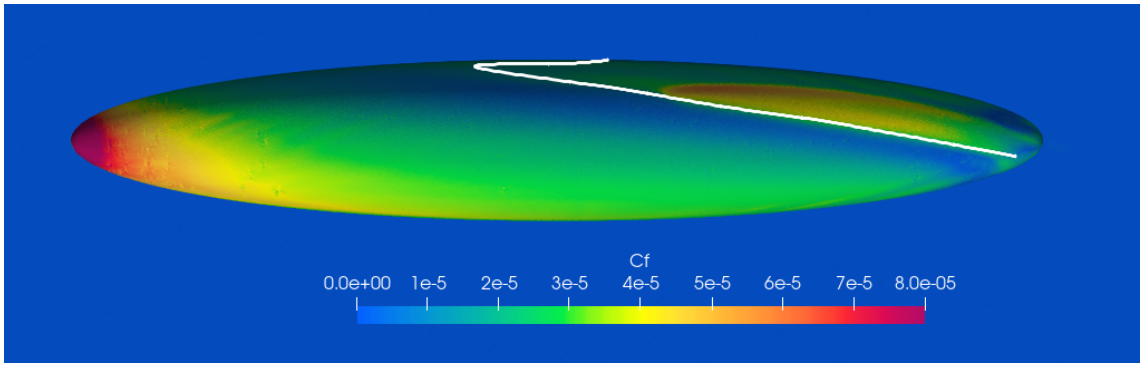

Figure 3. Skin friction coefficient contours for Case B.

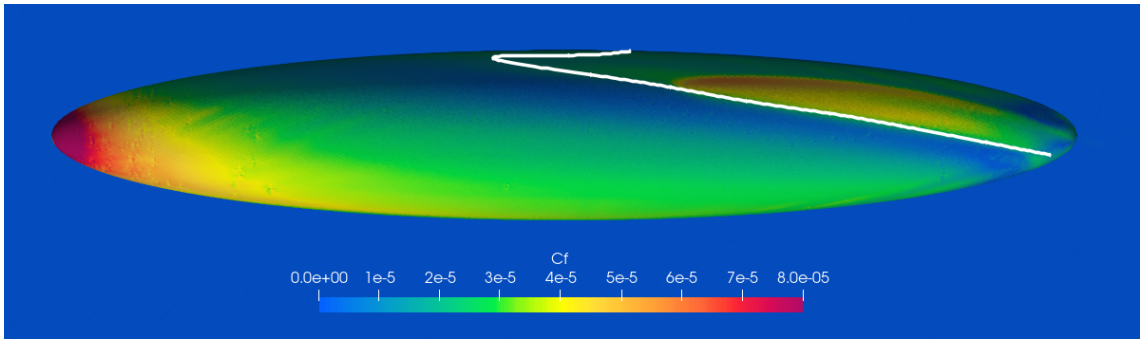

Figure 4. Skin friction coefficient contours for Case C.

attack, and 6.5×10^6 Reynolds number in the tunnel experiments for transition due to crossflow instabilities. However, in the experimental results the surface roughness was not quoted (Langtry *et al.*, 2015), and the freestream turbulence intensity in the wind tunnel level was in the range of $Tu_\infty = 0.1\%$. The result is confronted with the numerical results the c_f contours for stationary crossflow transition found in Langtry *et al.* (2015). The transition front extracted from the reference results is indicated in the following figures by the yellow line in our plots of c_f.

In Langtry *et al.* (2015), the authors considered a flow condition with a 6.5 million Reynolds number, an angle of attack of 15 degrees, Tu_i of 0.1%, and a surface roughness of 3.3μm. The authors obtained the results of c_f with the unstructured BCFD code and with the OVERFLOW code. According to Langtry *et al.* (2015), they observed an early transition for the results with the OVERFLOW code, but good agreement with the experimental data. To summarize, Table 2 presents the reference flow conditions of the test cases for the freestream turbulence intensity, Tu_i, an eddy viscosity to

molecular viscosity ratio, μ_t/μ_{ref}, the surface roughness, h, and the mesh nodes total number.

Table 2. Freestream turbulent variables for stationary crossflow vortices test case.

Case	Re	Mach	α	T_u	μ_t/μ_{ref}	h(μm)	Mesh(Total nodes)
Case A	6.5×10^6	0.14	15 deg	0.1%	10	3.3	2,715,698
Case B	6.5×10^6	0.14	15 deg	0.1%	10	3.3	8,949,137

Figures 5 and 7 depict the c_f contours. The region on the surface where the contours shift from blue to red represents the transition location. Case A, represented in Fig. 5, stands for the numerical results of c_f for the coarse mesh. We observe some discrepancies between our numerical results and the yellow line, which represents the results available in Langtry *et al.* (2015), as mentioned before. The main discrepancy is in the form and location of the transition. Figure 6 shows the residual convergence for the L-infinity norm for the four turbulent variables, k, ω, γ, and Re_{θ_t} for the results shown in Fig. 5. As previous indicated, this test consists of transition caused by crossflow instabilities. It is possible to see that the equation for γ and both equations for the SST model, k and ω, have similar convergence rates. However, the equation for Re_{θ_t} has the lower convergence rate.

Case B, represented in Fig.7, shows c_f contours for the fine mesh. We also observe some discrepancy in the transition location and form, as well as in the previous results even for the fine mesh. Currently, additional tests are being performed in order to fully understand the numerical results obtained with the BRU3D code. We understand that numerical characteristics of a particular code can lead to variations in the computational results. Also, the addition of new nonlineatiries from the new equations can influence the numerical results from solver to solver, and further investigation is being performed.

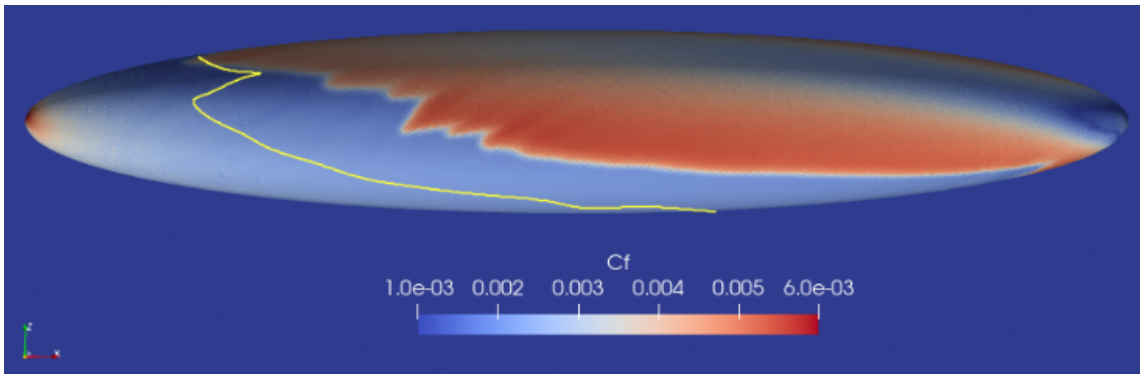

Figure 5. Skin friction coefficient contours obtained for Case A with crossflow effects for the course mesh.

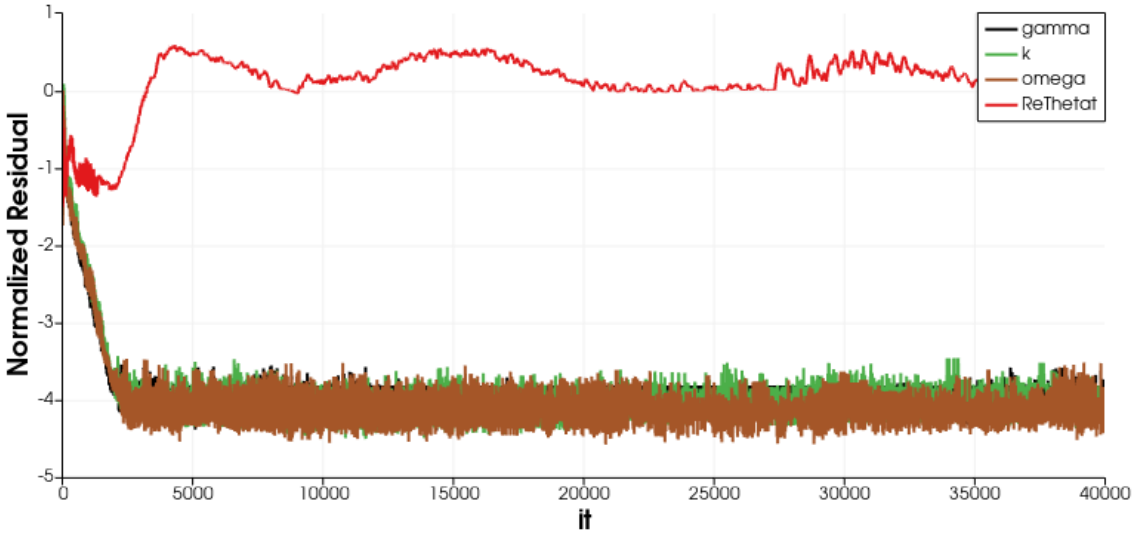

Figure 6. Residual convergence for crossflow-triggered transition for Case A.

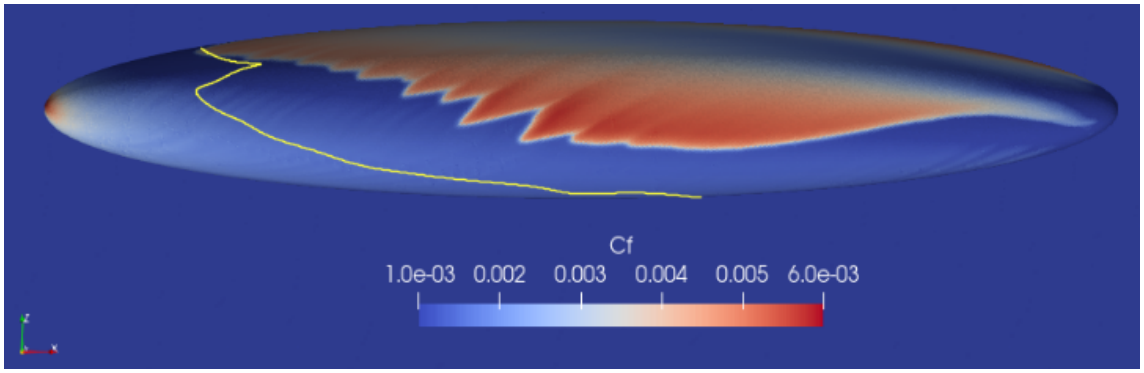

Figure 7. Skin friction coefficient contours obtained for Case B with crossflow effects for the fine mesh.

4. CONCLUSIONS

In the present study, two versions of the Langtry-Menter transition model are implemented in an in-house code, BRU3D. The first model implemented accounts for transition due to the amplification of Tollmien-Schlichting waves and bypass transition. The second implementation considers the extended model with an empirical correlation accounting for transition due to stationary crossflow vortices. In a previous work, the code is tested for a flat plate test case considering transition caused by Tollmien-Schlichting waves and bypass transition, and for the NLF(1)-0416 airfoil test case caused by Tollmien-Schlichting waves. The present study includes the prolate spheroid test case, which is a well-known case for transition caused by stationary crossflow vortices. We confront our numerical results with experimental values available in the literature, and we observe good agreement. Three cases for three different freestream turbulence intensity values are investigated. Comparing the three cases, we observe that for Cases B and C the c_f values and levels are slightly lower than the c_f values and levels for Case A. We also present a residual convergence for the four turbulent variables.

The empirical correlation for stationary crossflow vortices was implemented in the BRU3D code. We start our investigations with a mesh refinement study for the same values of reference freestream variables. Case A considers a coarse mesh, and Case B is based on a fine mesh. We observe similar values for the c_f contours, but differences in the transition front format. We also report some discrepancies between our numerical results and the data available in the literature. However, we observe a transition front whose overall topology is similar to the results from other research groups. It is worth mentioning that the addition of the new equations for the crossflow effects leads to more nonlinearities in the code, and further investigations are being performed in order to fully understand our numerical results with the BRU3D code. Finally, we also present a study on the residual convergence for the four variables, where it is possible to observe the influence on the numerical convergence with the equations for the crossflow empirical correlation, resulting in overall higher levels of residuals for all turbulent properties.

5. ACKNOWLEDGEMENTS

The authors gratefully acknowledge the support provided by Fundação de Amparo à Pesquisa do Estado de São Paulo, FAPESP, through a doctoral scholarship for the first author under Grant No. 2021/00031-0. The simulations in the present work would not be possible without the computational resources from the Center for Mathematical Sciences Applied to Industry (CeMEAI), funded by FAPESP under the Research Grant No. 2013/07375-0. Additional support to the third author under the FAPESP Research Grant No. 2013/07375-0 is also gratefully acknowledged. Further support for the present research was provided by Conselho Nacional de Desenvolvimento Científico e Tecnológico, CNPq, under the Research Grant No. 309985/2013-7.

6. REFERENCES

Bigarella, E.D.V., 2007. *Advanced Turbulence Modelling for Complex Aerospace Applications*. Ph.D. thesis, Instituto Tecnológico de Aeronáutica, São José dos Campos, Brazil.

Bigarella, E.D.V. and Azevedo, J.L.F., 2007. "Advanced eddy-viscosity and Reynolds-stress turbulence model simulations of aerospace applications". *AIAA Journal*, Vol. 45, No. 10, pp. 2369–2390.

Bigarella, E.D.V. and Azevedo, J.L.F., 2009. "A unified implicit CFD approach for turbulent-flow aerospace-configurations simulations". In *Proceedings of the 47th AIAA Aerospace Sciences Meeting Including the New Horizons Forum and Aerospace Exposition*. Orlando, FL.

Carvalho, L.M.M.O., 2018. *Numerical Study of Transitional Flows Over Aerospace Configurations*. Master's thesis, Instituto Tecnológico de Aeronáutica, São José dos Campos, Brasil.

Carvalho, L.M.M.O., da Silva, R.G. and Azevedo, J.L.F., 2018. "Numerical study of transitional flows over aerospace

configurations". In AIAA Paper No. 2018-4209*, Proceedings of the 2018 AIAA Applied Aerodynamics Conference, AIAA Aviation Forum*. doi:10.2514/6.2018-4209.

Coder, J.G., 2018. "Standard test cases for transition model verification and validation in computational fluid dynamics". In AIAA Paper No. 2018-0029*, Proceedings of the 2018 AIAA Aerospace Sciences Meeting, AIAA SciTech Forum*. Kissimmee, FL. doi:10.2514/6.2018-0029.

Ghasemi, E., McEligot, D., Nolan, K., Crepeau, Siahpush, A., Budwig, R. and Tokuhiro, A., 2014. "Effects of adverse and favorable pressure gradients on entropy generation in a transitional boundary layer region under the influence of freestream turbulence". *International Journal of Heat and Mass Transfer*, Vol. 77, pp. 475–488.

Grabe, C. and Krumbein, A., 2013. "Transition transport modeling for three-dimensional aerodynamic configurations". *Journal of Aircraft*, Vol. 50, No. 5, pp. 1535–1539. doi:10.2514/1.C032063.

Halila, G.L.O., 2014. *A Numerical Study on Transitional Flows by Means of a Correlation-Based Transition Model*. Ph.D. thesis, Instituto Tecnológico de Aeronáutica, São José dos Campos, Brazil.

Halila, G.L.O., Bigarella, E.D.V. and Azevedo, J.L.F., 2016. "A numerical study on transitional flows using a correlation-based transition model". *Journal of Aircraft*, Vol. 53, No. 4, pp. 922–941. doi:10.2514/1.C033311.

Halila, G.L.O., Chen, G., Shi, Y., Fidkowski, K.J., Martins, J.R.R.A. and Mendonça, M., 2019. "High-Reynolds number transitional flow prediction using a coupled discontinuous-Galerkin RANS PSE framework". *Aerospace Science and Technology*, Vol. 91, pp. 321–336. doi:10.1016/j.ast.2019.05.018.

Hirsh, C., 1990. *Numerical Computation of Internal and External Flows*. Wiley.

Jones, W. and Launder, B.E., 1973. "The calculation of low reynolds number phenomena with a two-equation model of turbulence". *International Journal of Heat and Mass Transfer*, Vol. 6, pp. 1119–1130.

Klebanoff, P.S., Tidstrom, K.D. and Sargent, L.M., 1962. "The three-dimensional nature of boundary layer instability". *Journal of Fluid Mechanics*, Vol. 12, pp. 1–24.

Kreplin, H.P., Vollmers, H. and Meier, H.U., 1985. "Wall shear stress measurements on an inclined prolate spheroid in the dfvlr 3m x 3m low speed wind tunnel, göttingen". Technical Report IB-22-84-A-33, DFVLR-AVA.

Langtry, R.B., Sengupta, K., Yeh, D.T. and Dorgan, A.J., 2015. "Extending the γ - Re local correlation based transition model for crossflow effects". In *Proceedings of the 2015 AIAA Fluid Dynamics Conference, AIAA Aviation Forum,* AIAA Paper No. 2015-2474. Dallas, TX. doi:10.2514/6.2015-2474.

Langtry, R.B. and Menter, F.R., 2009. "Correlation-based transition modeling for unstructured parallelized computational fluid dynamics codes". *AIAA Journal*, Vol. 47, No. 12, pp. 2894–2906.

Menter, F.R., 1994. "Two-equation eddy viscosity turbulence models for engineering applications". *AIAA Journal*, Vol. 32, No. 8, pp. 1598–1605.

Poll, D.I.A., 1978. "Some aspects of the flow near a swept attachment line with particular reference to boundary layer transition". College of Aeronautics TR 7805, College of Aeronautics, Cranfield, England, UK.

Righi, A.R.S., Carvalho, L.M.M.O., Halila, G.L.O. and Azevedo, J.L.F., 2021. "A numerical study on the effects of mesh refinament, artificial dissipation, and freestream turbulence on laminar-turbulent transition predictions". In *Proceedings of the 26th International Congress of Mechanical Engineering, COBEM-2021*. Virtual Congress, Brazil.

Rumsey, C.L. and Lee-Rausch, E.M., 2015. "NASA trapezoidal wing computations including transition and advanced turbulence modeling". *Journal of Aircraft*, Vol. 52, pp. 496–509.

Saric, W.S. and Dagenhart, J.R., 1999. "Crossflow stability and transition experiments in swept-wing flow". NASA TP-1999-209344, NASA.

Savill, A.M., 1993. "Some recent progress in the turbulence modeling of by-pass". In *Near-Wall Turbulent Flows, Elsevier*. pp. 829–848.

Savill, A.M., 1996. *One-Point Closures Applied to Transition, Turbulence and Transition Modeling*. edited by M. Hallbäck, Kluwer, Dordrecht.

Slotnick, J., Khodadoust, A., Alonso, J., Darmofal, D., Gropp, W., Lurie, E. and Mavriplis, D., 2014. "CFD vision 2030 study: A path to revolutionary computational aerosciences". NASA CR–2014-218178, NASA.

Smith, A.M.O. and Gamberoni, N., 1956. "Transition, pressure gradient and stability theory". Douglas Aircraft Company Report ES 26388, Douglas Aircraft Company, Long Beach, CA.

Somers, D.M., 1981. "Design and experimental results for a natural-laminar-flow airfoil for general aviation applications". Technical Report NASA TP-1681, National Aeronautics and Space Administration – NASA.

van Ingen, L.J., 1956. "A suggested semi-empirical method for the calculations of the boundary layer transition region". Dept. Aerospace Engineering VTH 74, University of Delft, Delft, The Netherlands.

7. RESPONSIBILITY NOTICE

The authors are the only responsible for the printed material included in this paper.